THE JOURNAL OF PHYSICAL CHEMISTRY B

Article

pubs.acs.org/JPCB

Influence of Sodium Cationization versus Protonation on the Gas-Phase Conformations and Glycosidic Bond Stabilities of 2′-Deoxyadenosine and Adenosine

Y. Zhu,[†] L. A. Hamlow,[†] C. C. He,[†] S. F. Strobehn,[†] J. K. Lee,[†] J. Gao,[‡] G. Berden,[‡] J. Oomens,[‡] and M. T. Rodgers*[,†]

[†]Department of Chemistry, Wayne State University, Detroit, Michigan 48202, United States

[‡]Radboud University, Institute for Molecules and Materials, FELIX Laboratory, Toernooiveld 7c, 6525ED Nijmegen, The Netherlands

Supporting Information

ABSTRACT: The influence of noncovalent interactions with a sodium cation on the gas-phase structures and N-glycosidic bond stabilities of 2′-deoxyadenosine (dAdo) and adenosine (Ado), $[dAdo+Na]^+$ and $[Ado+Na]^+$, are probed via infrared multiple photon dissociation (IRMPD) action spectroscopy and energy-resolved collision-induced dissociation (ER-CID) experiments. ER-CID experiments are also performed on the protonated forms of these nucleosides, $[dAdo+H]^+$ and $[Ado+H]^+$, for comparison purposes. Complementary electronic structure calculations are performed to determine the structures and relative stabilities of the stable low-energy conformations of the sodium cationized nucleoside complexes and to predict their IR spectra. Comparison between the measured IRMPD action spectra and calculated IR spectra enables the conformations of the sodium cationized nucleosides present in the experiments to be elucidated. The influence of sodium cationization versus protonation on the structures and IR spectra is elucidated by comparison to IRMPD and theoretical results previously reported for the protonated forms of these nucleosides. The influence of sodium cationization versus protonation on the glycosidic bond stability of the adenine nucleosides is determined by comparison of the ER-CID behavior of these systems. All structures present in the experiments are found to involve tridentate binding of Na^+ to the N3, O4′, and O5′ atoms forming favorable 5- and 6-membered chelation rings, which requires that adenine rotate to a *syn* configuration. This mode of sodium cation binding results in moderate flexibility of the sugar moiety such that the sugar puckering of the conformations present varies between C2′-endo and O4′-endo. Sodium cationization is found to be less effective toward activating the N-glycosidic bond than protonation for both dAdo and Ado. Both the IRMPD yields and ER-CID behavior indicate that the 2′-hydroxyl substituent of Ado stabilizes the N-glycosidic bond relative to that of dAdo.

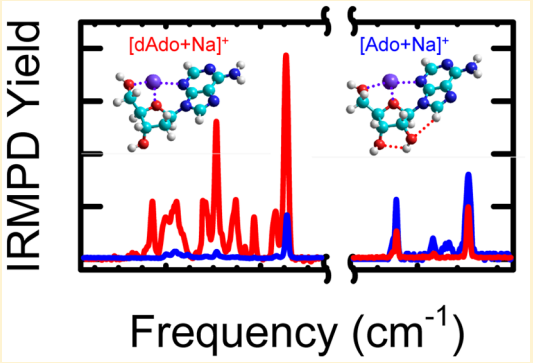

INTRODUCTION

Although chemically similar, DNA and RNA nucleic acids generally exhibit very different 2°, 3°, and 4° structures. DNA is most often found as a B form right-handed double helix with the nucleobases in an *anti* orientation and the 2′-deoxyribose sugar moieties exhibiting C2′-endo puckering, which is stabilized by Watson−Crick base pairing and π-stacking interactions. However, DNA is highly polymorphic and can take on a variety of other double-stranded structures including the A and Z forms[1,2] as well as triple- and quadruple-stranded structures by altering the base pairing, π-stacking, sugar puckering, and the direction and periodicity of the helix. In contrast, RNA generally exists as a single-stranded structure with the nucleobases in an anti orientation and the ribose sugar moieties exhibiting C3′-endo puckering, which is also stabilized by Watson−Crick base pairing achieved by folding back on itself to create helices, loops, bulges, and junctions. The structures of nucleic acids are also influenced by interactions with metal cations, protons, water, a wide variety of ligands, proteins, enzymes, and other nucleic acids. Indeed, interactions with metal cations and protons lead to the stabilization of both canonical and noncanonical structures, whereas interactions with the latter species are the means by which nucleic acids perform their various functions.[3,4] In order to better understand and manipulate the structures and functional properties of more complex DNA and RNA polymers, studies of the DNA and RNA nucleosides and how their structures and stabilities are influenced by the local environment are of fundamental importance.[5−12] Sodium cations participate in biological processes via noncovalent interactions with DNA and RNA

Received: June 16, 2016
Revised: August 2, 2016
Published: August 5, 2016

DOI: 10.1021/acs.jpcb.6b06105
J. Phys. Chem. B 2016, 120, 8892−8904

nucleic acids. At low concentrations, sodium cations bind to the phosphate groups along the backbone due to their negative charges.[3] At higher concentrations, sodium cations may interact with the nucleobase and/or sugar moieties and disrupt hydrogen bond base pairing, and thus alter the structural integrity of the nucleic acid polymer. Free and protein-bound sodium cations affect synthesis, replication, and cleavage of DNA and RNA.[4] In particular, alkali metal cations stabilize and prevent transitions from the B form of DNA.[13]

Sodium cations are also involved in nucleoside transport. On the basis of the primary mechanism of transport, the nucleoside transporters fall into two categories, equilibrative nucleoside transporter (ENT) and concentrative nucleoside transporter (CNT).[14] The driving force in equilibrative transport is the nucleoside concentration gradient, whereas, in concentrative transport, the nucleosides couple to a sodium cation, which generates an electrochemical ion gradient to drive cellular nucleoside uptake against their concentration gradients. CNT1 exhibits high selectivity for transfer of pyrimidine nucleosides and adenosine in a Na^+-dependent manner with high affinities. However, the transport efficiency of adenosine by CNT1 is much lower than those of the pyrimidine nucleosides.[15−17] For rat CNT1, the sodium cation:nucleoside ratio was determined to be 1:1.[16] CNT2 selectively transports purine nucleosides and uridine with high affinities. However, the transport efficiency of uridine by recombinant human CNT2 is relatively lower than that for purine nucleosides.[18,19] CNT3 transports both pyrimidine and purine nucleosides, and utilizes electrochemical gradients of either sodium cations or protons to accumulate nucleosides within cells.[20−24] Unlike CNT1 and CNT2, which exhibit a 1:1 Na^+:nucleoside coupling ratio, CNT3 employs a 2:1 coupling ratio.[25]

2′-Deoxyadenosine (dAdo) and adenosine (Ado) are fundamental building blocks of DNA and RNA nucleic acids, respectively. The chemical structures of dAdo and Ado are shown in Figure 1. 2′-Deoxyadenosine has been found to play an important role in adenosine deaminase (ADA) deficiency, which causes severe combined immunodeficiency disease of infancy and childhood.[26,27] A low concentration of dAdo can lead to the selective lymphopenia observed in ADA deficient patients.[28,29] Adenosines play important roles in biochemical processes as the nucleoside of adenosine-5′-triphosphate (ATP) and adenosine-5′-diphospate (ADP), which act as energy carriers in cells, and of 3′,5′-cyclic adenosine monophosphate (cAMP), which serves as a secondary messenger of intracellular signal transduction.[30,31] Extracellular Ado is generated from the conversion of extracellular ATP[32−34] and extracellular cAMPs.[35,36] Adenosine is also an anti-inflammatory that is elevated by extracellular guanosine, which increases under conditions of cell injury.[37]

In this study, a custom-built Fourier transform ion cyclotron resonance mass spectrometer (FT-ICR MS) coupled to a wavelength tunable IR laser is used to perform infrared multiple photon dissociation (IRMPD) action spectroscopy experiments for $[dAdo+Na]^+$ and $[Ado+Na]^+$. Complementary electronic structure calculations are performed to determine the stable low-energy conformations of these complexes and to predict their IR spectra. Comparative analyses of the measured IRMPD action spectra and computed linear IR spectra enable the conformations accessed in the experiments to be elucidated. This methodology has proven to be an effective way to characterize the gas-phase conformations and energetics of deprotonated, protonated, and sodium cationized nucleobases,[38−45] nucleosides,[5−9,46,47] and nucleotides.[48−55] All favorable modes of sodium cation binding, adenine orientation, and sugar puckering are comprehensively examined to better understand the influence of noncovalent interactions with sodium cations on the structures and relative stabilities of $[dAdo+Na]^+$ and $[Ado+Na]^+$. Comparisons to results from analogous IRMPD studies of the protonated forms of 2′-deoxyadenosine, $[dAdo+H]^+$, and adenosine, $[Ado+H]^+$, enable the effects of protonation vs sodium cationization on structure to be determined. Energy-resolved collision-induced dissociation (ER-CID) experiments of the sodium cationized and protonated forms of 2′-deoxyadenosine, $[dAdo+Na]^+$ and $[dAdo+H]^+$, and adenosine, $[Ado+Na]^+$ and $[Ado+H]^+$, are also performed using a Bruker amaZon ETD quadrupole ion trap mass spectrometer (QIT MS). Survival yields as a function of the radio frequency (rf) excitation voltage are measured and fitted to characterize the relative stabilities of the sodium cationized and protonated adenine nucleosides. Trends in the energetics of dissociation are examined to elucidate the relative abilities of sodium cations vs protons for activating the N-glycosidic bonds of dAdo and Ado, and to determine the influence of the 2′-hydroxyl substituent on N-glycosidic bond stability.

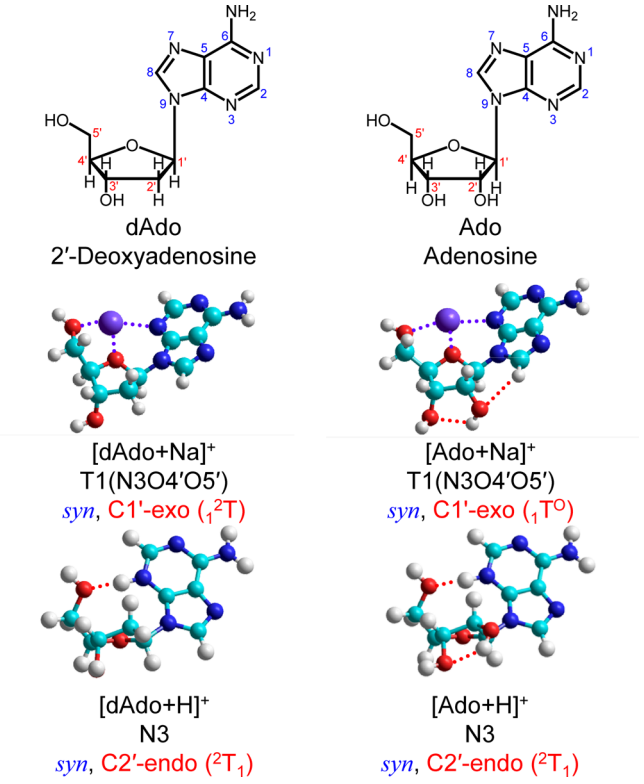

Figure 1. Chemical structures of 2′-deoxyadenosine and adenosine. The ground-state structures of $[dAdo+Na]^+$ and $[Ado+Na]^+$ predicted at the B3LYP/6-311+G(2d,2p)//B3LYP/6-311+G(d,p) level of theory. The sodium cation binding mode, nucleobase orientation, and sugar configuration are also given for each structure. The B3LYP/6-311+G(2d,2p)//B3LYP/6-311+G(d,p) ground-state structures of $[dAdo+H]^+$ and $[Ado+H]^+$ taken from ref 6 are also shown for comparison. The preferred site of protonation, nucleobase orientation, and sugar configuration are also indicated.

DOI: 10.1021/acs.jpcb.6b06105
J. Phys. Chem. B 2016, 120, 8892−8904

EXPERIMENTAL AND COMPUTATIONAL SECTION

Chemical Reagents. The ER-CID experiments were performed at Wayne State University. The adenine nucleosides (dAdo and Ado), sodium chloride (NaCl), methanol, and water were purchased from Sigma-Aldrich (St. Louis, MO, USA). Acetic acid was purchased from Mallinckrodt Chemicals (St. Louis, MO, USA). The IRMPD action spectroscopy experiments were performed at the FELIX facility at Rabdoud University. The adenine nucleosides were shipped from Wayne State University. Sodium chloride (NaCl), methanol, and water were purchased from Sigma-Aldrich (Zwijndrecht, The Netherlands).

FT-ICR MS and Wavelength-Dependent Photodissociation. IRMPD action spectra of $[dAdo+Na]^+$ and $[Ado+Na]^+$ were measured using a custom-built 4.7 T FT-ICR MS coupled to the free-electron laser for infrared experiments (FELIX)[56] or a Nd:YAG-pumped (Innolas Spitlight 600) optical parametric oscillator laser system (OPO, LaserVision, Bellevue, WA). The $[dAdo+Na]^+$ or $[Ado+Na]^+$ complexes were generated from solutions containing 1 mM dAdo or Ado and 1 mM NaCl in 90%:10% to 50%:50% (v/v) methanol (MeOH):water (H_2O) mixtures by direct infusion at a flow rate of 2−5 μL/min into a Micromass "Z-Spray" electrospray ionization (ESI) source. Ions emanating from the ESI source were accumulated in a rf hexapole ion trap for several seconds to enhance signal-to-noise and affect efficient thermalization of the ions, pulse extracted through a quadrupole bender, and injected into the ICR cell through an rf octopole ion guide.[57] The sodium cationized nucleoside, $[dAdo+Na]^+$ or $[Ado+Na]^+$, was isolated using stored waveform inverse Fourier transform (SWIFT) techniques and subsequently irradiated by the FEL or OPO laser to induce IR photodissociation. The output power of the FEL enables efficient IRMPD in 3 s, whereas the reduced output of the OPO laser requires 8.5 s to achieve similar dissociation efficiency. The IRMPD behavior is examined over the ranges between ∼550 and 1850 cm^{-1} (FELIX) and between ∼3300 and 3800 cm^{-1} (OPO). Further details regarding the experimental setup are provided elsewhere.[58,59]

QIT MS and Energy-Resolved Collision-Induced Dissociation. Energy-resolved collision-induced dissociation (CID) experiments of the protonated and sodium cationized forms of the adenine nucleosides, $[dAdo+H]^+$, $[Ado+H]^+$, $[dAdo+Na]^+$, and $[Ado+Na]^+$, were performed using a Bruker amaZon ETD QIT MS. The commercial QIT MS instrument is much more sensitive than the custom-built FT-ICR MS such that the protonated and sodium cationized nucleosides were generated from solutions containing 10 μM dAdo or Ado in a 50%:50% MeOH:H_2O mixture at a flow rate of 3 μL/min. Addition of 1% (v/v) acetic acid was used to promote production of the protonated species, whereas 10 μM NaCl was used to promote formation of the sodium cationized species. Ions were transferred into a dual rf ion funnel after exiting the glass capillary. After exiting the second ion funnel through a small aperture, ions were guided using a high-precision rf hexapole, and accumulated in the ion trap where CID experiments were performed. Helium buffer gas was introduced into the ion trap at a pressure of ∼1 mTorr for efficient trapping and cooling of the ions. The helium buffer gas also serves as the collision gas for the CID experiments. The q_z value was set to 0.25 for ion trapping and efficient CID experiments. As a consequence, the low mass cut-off for the CID experiments was 27% of the precursor ion mass. The fragmentation time, corresponding to the amount of time the resonant rf excitation was applied to excite the ion of interest, was set to 40 ms, corresponding to roughly 4000 collisions per ion. This time was chosen on the basis of control experiments where it was found that the fragmentation behavior achieves pseudoequilibrium conditions within 10−30 ms such that the fragmentation efficiency is no longer related to the fragmentation time. The rf excitation amplitude was varied from 0 V to the amplitude required to produce complete fragmentation of the precursor ion at a step size of 0.01 V. Experiments were performed in triplicate to assess reproducibility of the measurements. Data analysis was performed using Compass Data Analysis 4.0 (Bruker Daltonics, Bremen, Germany) and SigmaPlot 10.0 (Systat Software, Inc., San Jose, CA, USA).

Computational Details. The chemical structures of neutral dAdo and Ado are displayed in Figure 1. In order to obtain low-energy candidate structures for the sodium complexes of these nucleosides, simulated annealing procedures were performed followed by density functional theory (DFT) calculations. Simulated annealing was performed using the HyperChem[60] software package with the Amber 3 force field. A variety of initial structures were built and subjected to simulated annealing to comprehensively examine the various favorable Na^+ binding modes of the nucleobase moiety that are available to these adenine nucleosides. In particular, binding to the adenine nucleobase at the N1, N3, and N7 positions was examined. Each candidate sodium cationized nucleoside structure was subjected to 300 cycles of annealing. Each cycle involved four steps: (1) 0.3 ps of thermal heating ramped linearly from 0 to 1000 K, (2) sampling of conformational space at the simulation temperature, 1000 K, for 0.2 ps, (3) thermal cooling via a linear decrease in temperature back down to 0 K over a period of 0.3 ps, and (4) optimization of the resultant structure to a local minimum. A molecular mechanics calculation was performed every 1 fs in each cycle, and a snapshot of the lowest energy structure at the end of each cycle was saved and used as the starting structure for the next cycle of simulated annealing. Structures from among the 900 snapshots produced by simulated annealing for each nucleoside complex were chosen for DFT optimization and energetic characterization on the basis of their relative stabilities determined via the molecular mechanics optimization. Geometry optimization and harmonic vibrational frequency calculations were performed at the B3LYP/6-311+G(d,p) level of theory using the Gaussian 09 suite of programs.[61] In order to determine the relative stabilities of the stable low-energy conformers of $[dAdo+Na]^+$ and $[Ado+Na]^+$, single point energies were calculated at the B3LYP/6-311+G(2d,2p) level of theory. In order to better reproduce the measured IRMPD spectra, the vibrational frequencies in the FELIX region are scaled by 0.9794 and broadened using a 20 cm^{-1} fwhm Gaussian line shape, whereas vibrational frequencies in the OPO region are scaled by 0.9558 and broadened using a 15 cm^{-1} fwhm Gaussian line shape.

RESULTS

IRMPD Action Spectroscopy. Three photodissociation pathways are observed for the sodium cationized adenosine nucleosides as summarized in reactions 1−3,

$$[Nuo+Na]^+ + n\,h\nu \rightarrow Na^+ + Nuo \quad (1)$$

DOI: 10.1021/acs.jpcb.6b06105
J. Phys. Chem. B 2016, 120, 8892−8904

$$[\text{Nuo+Na}]^+ + n\,h\nu \rightarrow [\text{Ade+Na}]^+ + [\text{Nuo−Ade}] \quad (2)$$

$$[\text{Nuo+Na}]^+ + n\,h\nu \rightarrow [\text{Nuo−Ade+Na}]^+ + \text{Ade} \quad (3)$$

where Nuo is either dAdo or Ado and Ade is adenine. Reaction 1 is simple noncovalent bond cleavage resulting in loss of the intact nucleoside. Reactions 2 and 3 correspond to glycosidic bond cleavage with the sodium cation retained either by the nucleobase or sugar moiety, respectively. All three photodissociation pathways are observed for $[\text{dAdo+Na}]^+$ in the FELIX region, whereas only reaction 2 is seen in the OPO region. In contrast, the only photodissociation pathway observed for $[\text{Ado+Na}]^+$ is the loss of the intact nucleoside, reaction 1, in both the FELIX and OPO regions. Absence of the glycosidic bond cleavage pathways in the experiments for $[\text{Ado+Na}]^+$ in the FELIX region results in much lower IRMPD yields than those observed for $[\text{dAdo+Na}]^+$ (see Figure 2).

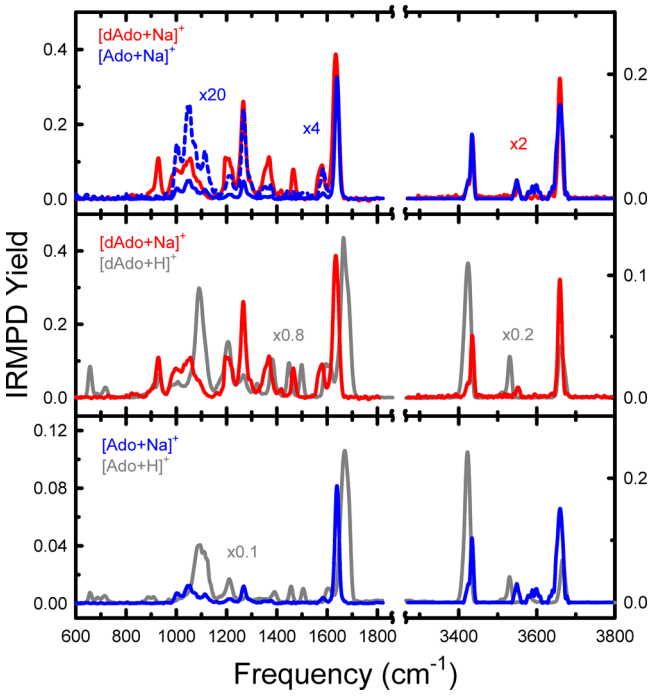

Figure 2. IRMPD action spectra of $[\text{dAdo+Na}]^+$ and $[\text{Ado+Na}]^+$ in the FELIX and OPO regions. IRMPD action spectra of $[\text{dAdo+H}]^+$ and $[\text{Ado+H}]^+$ previously reported are overlaid in gray for comparison.

Absence of the glycosidic bond cleavage pathways also suggests that the glycosidic bond of Ado is stronger than that of dAdo, consistent with that found in the energy-resolved CID studies performed here (and discussed below) and recent threshold CID studies of the protonated adenine nucleosides.[62] Parallel behavior is also found in analogous TCID studies of the protonated cytosine and guanine nucleosides, where the RNA nucleosides are found to exhibit stronger glycosidic bonds than the analogous DNA nucleosides.[63,64] The IRMPD yield was calculated using eq 4, where the fragment intensities (I_f) in all channels are summed and divided by the total ion intensity.

$$\text{IRMPD Yield} = (\sum_i I_{f_i})/(I_p + \sum_i I_{f_i}) \quad (4)$$

Data are reported as the IRMPD yield over the FELIX region for both complexes and over the OPO region for $[\text{dAdo+Na}]^+$. However, because of the weak Na^+ product signal in the OPO experiments for $[\text{Ado+Na}]^+$, the data are reported as the inverted depletion of the intensity of $[\text{Ado+Na}]^+$. Linear normalization with the FEL or OPO laser power is performed to correct for variations in the laser power as a function of photon energy. The IRMPD yield is plotted as a function of vibrational frequency from ∼550 to 1850 cm^{-1} and from ∼3300 to 3800 cm^{-1}. The measured IRMPD spectra of $[\text{dAdo+Na}]^+$ and $[\text{Ado+Na}]^+$ are compared in Figure 2 (note the different *y*-scaling of the IRMPD yield in the FEL (left) and OPO (right) regions). The IRMPD yield of $[\text{dAdo+Na}]^+$ in the FELIX region exceeds that of $[\text{Ado+Na}]^+$ (note the scaling factors used to facilitate comparisons). Comparisons in the OPO region are not straightforward, as the data for $[\text{Ado+Na}]^+$ is plotted as a depletion spectrum, whereas the data for $[\text{dAdo+Na}]^+$ is shown as the IRMPD yield. The measured IRMPD spectra of these two complexes are highly parallel except for the weak absorption at ∼3600 cm^{-1}, which is only observed for $[\text{Ado+Na}]^+$. The effect of the 2′-hydroxyl substituent is mainly observed in the IRMPD yields.

Energy-Resolved Collision-Induced Dissociation. Figure 3 shows the CID mass spectra of protonated and sodium

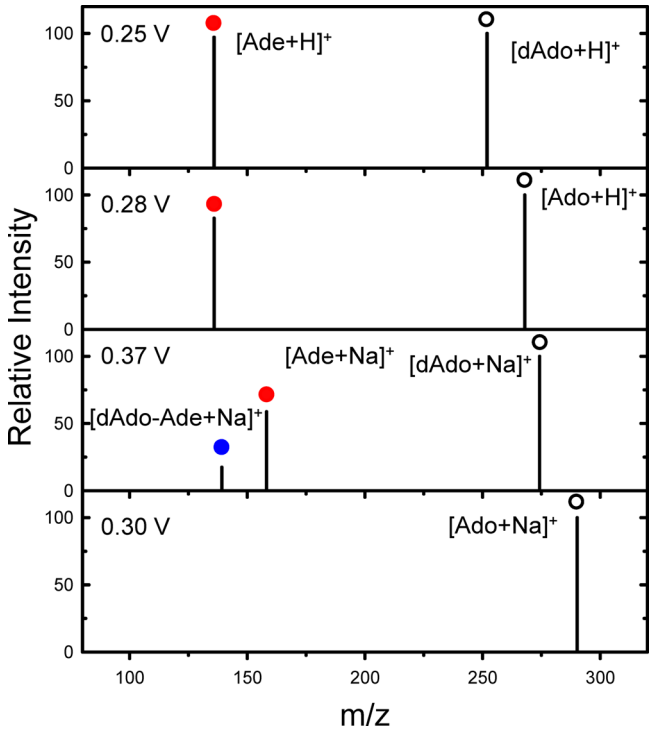

Figure 3. CID mass spectra of $[\text{dAdo+H}]^+$, $[\text{Ado+H}]^+$, $[\text{dAdo+Na}]^+$, and $[\text{Ado+Na}]^+$ at an rf excitation voltage producing ∼50% dissociation, corresponding to $CID_{50\%}$.

cationized dAdo and Ado at an rf excitation that produces ∼50% dissociation. For $[\text{dAdo+H}]^+$ and $[\text{Ado+H}]^+$, the only fragmentation pathway observed is glycosidic bond cleavage leading to the production of protonated adenine, analogous to reaction 2. For $[\text{dAdo+Na}]^+$, two fragmentation pathways are observed, both involving glycosidic bond cleavage with the sodium cation competitively retained by the adenine nucleobase or the sugar moiety, analogous to reactions 2 and 3. It is likely that reaction 1 also occurs but cannot be detected, as its ionic product, Na^+, has an *m*/*z* below the low-mass cutoff. In contrast, for $[\text{Ado+Na}]^+$, although the intensity of the

DOI: 10.1021/acs.jpcb.6b06105
J. Phys. Chem. B 2016, 120, 8892−8904

precursor ion decreases as the rf excitation voltage is increased, no CID products are observed. The lack of detectable CID products suggests that $[Ado+Na]^+$ undergoes CID solely by reaction 1, again indicating that the glycosidic bond of Ado is stronger than that of dAdo, as mentioned above. Clearly, these slow-heating methods, IRMPD and multiple-collision CID, produce similar activation and fragmentation behavior.

Survival Yield Analyses. In order to elucidate information regarding the relative stabilities of the protonated and sodium cationized adenine nucleosides, and in particular their relative glycosidic bond stabilities, survival yield analyses were performed.[65−68] The survival yield method is based on performing ER-CID (or in this case as a function of the applied rf excitation voltage) over the range of values required to bring about complete dissociation. The rf excitation voltage required to produce a survival yield of 50%, designated $CID_{50\%}$, is used for semiquantitative assessments of stability. Thus, comparison of the $CID_{50\%}$ values determined for the protonated and sodium cationized forms of dAdo and Ado provides a semiquantitative characterization of the relative stabilities. The survival yield is calculated as the ratio of the intensity of the precursor ion to the total ion intensity (i.e., the sum of the precursor and fragment ion intensities), as shown in eq 5.[69]

$$\text{Survival Yield} = I_p/(I_p + \sum_i I_{f_i}) \quad (5)$$

Results are reported as the average of three measurements (see Figure 4), where the error bars represent the standard deviation

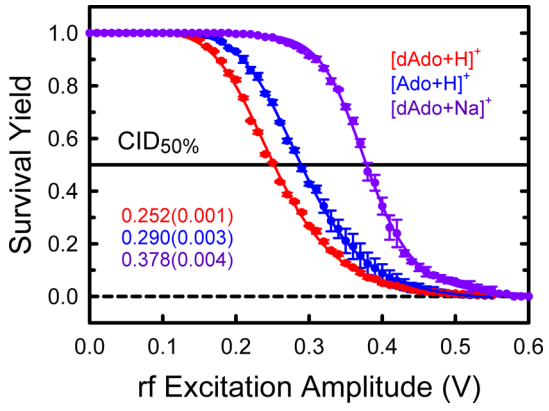

Figure 4. Survival yield analyses of $[dAdo+H]^+$, $[Ado+H]^+$, and $[dAdo+Na]^+$ and their corresponding $CID_{50\%}$ values.

of these three measurements. In order to extract $CID_{50\%}$ values for the protonated and sodium cationized forms of dAdo and Ado, each averaged survival yield curve was least-squares fit to the four parameter logistic curve of eq 6[69]

$$\text{Survival Yield} = \text{min} + \frac{\text{max} - \text{min}}{1 + (\text{rf EA}/\text{CID}_{50\%})^{\text{Hillslope}}} \quad (6)$$

where max and min are the maximum and minimum values of the survival yield, which are typically 1 and 0, respectively, rf EA is the rf excitation amplitude applied to induce fragmentation of the ion of interest, and Hillslope is the slope of the declining region of the survival yield curve and describes the steepness of the fall off of the data with increasing rf excitation.

Theoretical Results. The ground-state structures of $[dAdo+Na]^+$ and $[Ado+Na]^+$ optimized at the B3LYP/6-311+G(d,p) level of theory are shown in Figure 1. All stable low-energy conformers of $[dAdo+Na]^+$ and $[Ado+Na]^+$ found within 100 kJ/mol of the most stable structure computed for each nucleoside complex are shown in Figures S1 and S2 of the Supporting Information along with their B3LYP/6-311+G-(2d,2p) relative Gibbs free energies at 298 K. The relative stabilities of these low-energy conformers are highly dependent on the mode of sodium cation binding such that they are designated with a letter and a number, followed by the specific atoms that the sodium cation is bound to in parentheses. The letter is based on the number of chelation interactions between the sodium cation and nucleoside, T for tridentate, B for bidentate, and M for monodentate, whereas the number indicates the relative Gibbs free energy at 298 K of that conformer among all of the stable conformers that exhibit that same mode of sodium cation binding, with 1 for the most stable of these species, 2 for the next most stable, etc. In addition to being designated on the basis of the mode of sodium cation binding, the stable conformers are also designated on the basis of the nucleobase orientation and sugar puckering, as summarized in Figure S3 of the Supporting Information. The nucleobase orientation is defined on the basis of the ∠C4N9C1′O4′ dihedral angle, where values between −90° and 90° are designated as *syn* and values between 90° and 270° designated as *anti*. The sugar puckering is defined on the basis of the pseudorotation angle, *P*, of the sugar moiety as defined by Saenger[3] and in Figure S1. Two different sugar puckering designations are shown that are based on the more familiar, C2′-endo and C3′-endo, etc., designations and the somewhat less commonly employed, but more detailed, ^{2}E and ^{3}E, etc. designations.

In the ground conformers of the $[dAdo+Na]^+$ and $[Ado+Na]^+$ complexes, the sodium cation binds in a tridentate fashion to the N3, O4′, and O5′ atoms, forming 5- and 6-membered chelation rings, with adenine in a *syn* orientation and puckering of the sugar moieties that is approximately C1′-exo ($_1^2$T and $_1$T^0, respectively). Table 1 compares geometric details of these ground-state structures. Compared with $[dAdo+Na]^+$, the adenine moiety along with the sodium cation in $[Ado+Na]^+$ are rotated slightly such that the Na^+−N3 bond distance is essentially preserved and differs by only 0.001 Å, whereas the Na^+−O4′ bond length increases from 2.248 to 2.271 Å, the Na^+−O5′ bond length decreases slightly from 2.349 to 2.343 Å, and the ∠N3Na^+O5′ angle increases from

Table 1. Geometric Details of the B3LYP/6-311+G(d,p) Ground-State Conformers of $[dAdo+Na]^+$ and $[Ado+Na]^+$ [a]

		$[dAdo+Na]^+$	$[Ado+Na]^+$
bond length	Na^+···N3	2.345 Å	2.346 Å
	Na^+···O4′	**2.248 Å**	**2.271 Å**
	Na^+···O5′	**2.349 Å**	**2.343 Å**
	C1′···N9	**1.458 Å**	**1.448 Å**
	O2′H···O3′	-	**2.171 Å**
bond angle	∠N3Na^+O4′	81.2°	81.1°
	∠O4′Na^+O5′	71.2°	71.2°
	∠N3Na^+O5′	**144.1°**	**151.3°**
dihedral angle	∠C4N9C1′O4′	−44.1°	−46.4°
	∠O5′C5′C4′O4′	52.9°	53.9°

[a]Bond distances and angles that differ significantly and thus are influenced by the presence of the 2′-hydroxyl substituent are indicated in boldface.

DOI: 10.1021/acs.jpcb.6b06105
J. Phys. Chem. B 2016, 120, 8892−8904

Table 2. Relative Enthalpies and Free Energies of Select Stable Low-Energy Conformers of $[dAdo+Na]^+$ and $[Ado+Na]^+$ at 0 and 298 K in kJ/mol[a]

species	conformer	ΔH_0	ΔH_{298}	ΔG_{298}	adenine orientation	P	sugar puckering
$[dAdo+Na]^+$	T1(N3O4′O5′)	4.1	5.1	**0.0**	*syn*	144.6°	C1′-exo ($_1^2$T)
	T2(N3O4′O5′)	**0.0**	**0.0**	1.4	*syn*	103.3°	O4′-endo (^{O}T$_4$)
	B1(O4′O5′)	48.0	49.6	41.4	*syn*	14.5°	C3′-endo (^{3}T$_2$)
	B1(N7NH$_2$)	66.2	66.6	65.0	*anti*	173.2°	C2′-endo (^{2}T$_3$)
	B1(N3O3′)	66.3	67.1	66.4	*anti*	138.1°	C1′-exo ($_1$T^2)
	B1(N1NH$_2$)	74.5	75.0	73.1	*anti*	173.3°	C2′-endo (^{2}T$_3$)
	B7(N7NH$_2$)	79.5	80.6	75.7	*syn*	164.5°	C2′-endo (^{2}T$_3$)
	B1(N3O5′)	79.4	79.4	79.5	*anti*	289.2°	C1′-endo ($_O^1$T)
	B8(N1NH$_2$)	91.4	92.0	88.4	*syn*	171.0°	C2′-endo (^{2}T$_1$)
	M1(N3)	100.9	102.7	95.4	*anti*	9.1°	C3′-endo (^{3}T$_2$)
$[Ado+Na]^+$	T1(N3O4′O5′)	**0.0**	**0.0**	**0.0**	*syn*	113.5°	C1′-exo ($_1$T^O)
	T3(N3O4′O5′)	5.2	5.4	4.3	*syn*	139.2°	C1′-exo ($_1$T^2)
	B1(N3O2′)	20.3	19.8	19.7	*anti*	68.1°	C4′-exo ($_4$T^O)
	T1(N3O2′O3′)	36.4	37.3	36.0	*anti*	140.4°	C1′-exo ($_1$T^2)
	B1(N3O4′)	42.3	43.0	39.5	*syn*	172.0°	C2′-endo (^{2}T$_3$)
	B1(O4′O5′)	52.2	51.9	50.5	*anti*	147.3°	C2′-endo (^{2}T$_1$)
	B1(N7NH$_2$)	62.6	62.7	60.3	*anti*	168.0°	C2′-endo (^{2}T$_3$)
	B3(N7NH$_2$)	62.5	61.2	63.2	*syn*	159.0°	C2′-endo (^{2}T$_1$)
	B1(N1NH$_2$)	70.2	70.4	67.1	*anti*	170.6°	C2′-endo (^{2}T$_3$)
	B9(N1NH$_2$)	77.3	76.3	77.2	*syn*	161.6°	C2′-endo (^{2}T$_1$)
	B1(N7O5′)	84.6	83.5	86.1	*syn*	342.1°	C2′-exo ($_2$E)

[a]Energetics based on single-point energy calculations performed at the B3LYP/6-311+G(2d,2p) level of theory, including ZPE and thermal corrections based on the B3LYP/6-311+G(d,p) optimized structures and vibrational frequencies.

144.1 to 151.3°. The C1′−N9 glycosidic bond of $[dAdo+Na]^+$ is 1.458 Å, which decreases to 1.448 Å in $[Ado+Na]^+$, suggesting that the 2′-hydroxyl substituent slightly strengthens the glycosidic bond. Thus, the most significant difference associated with the presence of the 2′-hydroxyl substituent is the hydrogen-bonding interaction it enables between the 2′- and 3′-hydroxyls. The relative enthalpies at 0 and 298 K and Gibbs free energies at 298 K of select stable low-energy conformers of $[dAdo+Na]^+$ and $[Ado+Na]^+$ along with conformer designations are summarized in Table 2, whereas results for all stable structures are listed in Table S1 of the Supporting Information. The conformers listed are chosen to show the various binding modes with *anti* and *syn* orientations of the adenine moiety.

Sodium Cation Binding to N3. Both $[dAdo+Na]^+$ and $[Ado+Na]^+$ prefer a *syn* orientation of adenine, which enables chelation of the sodium cation by the N3, O4′, and O5′ atoms. These chelation interactions lead to relatively compact structures with puckering of the sugar moiety that varies between C2′-exo ($_2$E) and C3′-exo ($_3$E), with conformations exhibiting puckering between C2′-endo (^{2}E) and O4′-endo (^{O}E) being the most stable (see Figure S1). Conformers that bind via bidentate interaction with the N3 and O4′ atoms are ∼40 kJ/mol less stable, indicating that the chelation interaction with the O5′ atom is an important contributor to the binding. N3 cationized *anti*-oriented conformers of $[dAdo+Na]^+$ and $[Ado+Na]^+$ are much less stable, by >60 kJ/mol for dAdo and almost 20 kJ/mol for Ado. The 2′-hydroxyl substituent provides additional stabilization by chelating with the sodium cation and hydrogen bonding to the 3′- and 5′-hydroxyl substituents, and thus accounts for the large stability difference determined. Conformers that bind via monodentate interaction with the N3 atom are only found for $[dAdo+Na]^+$, and these conformers are >95 kJ/mol less stable than the ground conformer.

Sodium Cation Binding to N1 or N7. All stable conformers that bind to the N1 or N7 atoms also chelate with the amino substituent or the 5′-hydroxyl substituent. Both *anti* and *syn* orientations are found with the *anti* conformers favored over *syn*. The interaction between the sodium cation and the NH_2 substituent interrupts the conjugated structure of adenine, and changes the hybridization of the amino nitrogen from sp^2 to sp^3. Sodium cation chelation with N7 and O5′ is observed in both $[dAdo+Na]^+$ and $[Ado+Na]^+$. Monodentate conformers binding to the N1 atom are only observed for $[Ado+Na]^+$, and these conformers are >96 kJ/mol less stable.

Sodium Cation Binding to the Sugar. Bidentate binding of a sodium cation to the O4′ and O5′ atoms is observed in the B1(O4′,O5′) conformer of $[dAdo+Na]^+$ and the B1(O4′,O5′) and B2(O4′,O5′) conformers of $[Ado+Na]^+$. The stabilities of these conformers are computed to be >40 kJ/mol less favorable than their corresponding tridentate ground conformers. The additional 2′-hydroxyl substituent of $[Ado+Na]^+$ forms a hydrogen bond with the N3 atom of adenine and limits N-glycosidic bond rotation. Therefore, the missing interaction between the sodium cation and adenine leads to significant destabilization of this conformer.

Sugar Puckering. A variety of sugar puckering configurations are found among the stable conformers of $[dAdo+Na]^+$ and $[Ado+Na]^+$ that vary between C1′-endo (^{1}E) and C4′-endo (^{4}E); only O4′-exo ($_O$E) conformations are not found. The multiple chelation interactions that stabilize binding to Na^+ in the ground and low-energy conformers lead to relatively compact structures that preferentially induce puckering of the sugar that lies between C2′-endo (2E) and O4′-endo (^{O}E); see Figure S1.

Stable Conformers of $[dAdo+Na]^+$ vs $[Ado+Na]^+$. As evidenced by the structures of the ground and low-energy conformers shown in Figures S2 and S3, tridentate binding of the sodium cation to N3, O4′, and O5′ is the most favorable

DOI: 10.1021/acs.jpcb.6b06105
J. Phys. Chem. B 2016, 120, 8892−8904

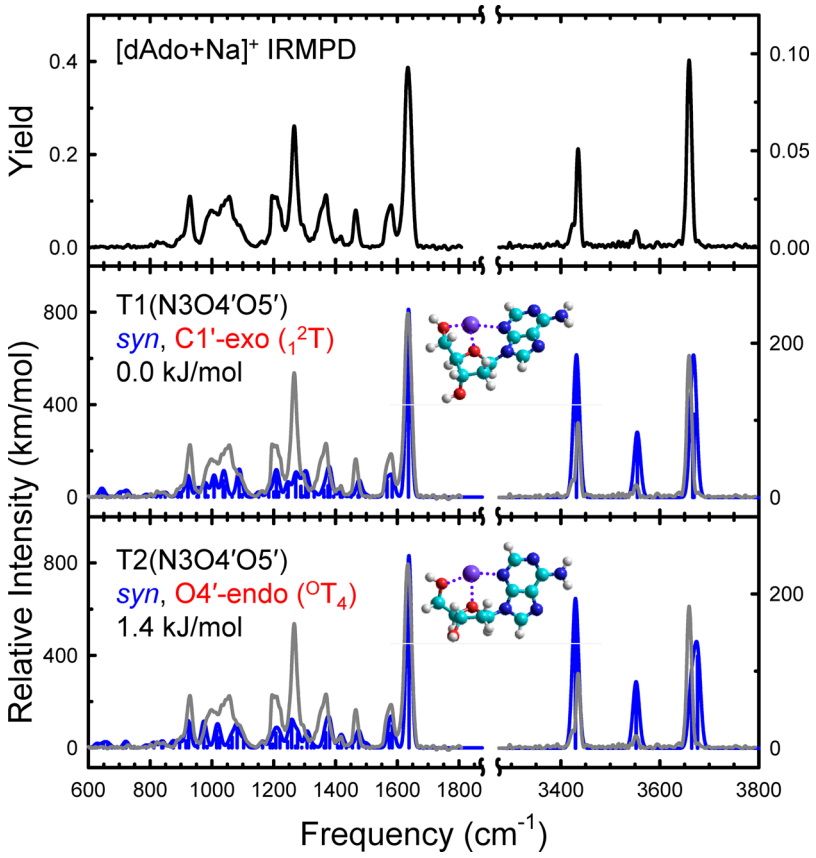

Figure 5. Comparison of the experimental IRMPD action spectrum of $[dAdo+Na]^+$ with the B3LYP/6-311+G(d,p) optimized structures and calculated linear IR spectra for the two low-energy conformers of $[dAdo+Na]^+$ that best match the measured spectrum. The adenine orientation, sugar configuration, and B3LYP/6-311+G(2d,2p) relative Gibbs free energies at 298 K are also shown.

mode of binding for both $[dAdo+Na]^+$ and $[Ado+Na]^+$. However, the 2′-hydroxyl substituent of $[Ado+Na]^+$ can chelate with the sodium cation or hydrogen bond with the nucleobase or sugar moieties to provide additional stabilization. Thus, bidentate conformers of $[Ado+Na]^+$ binding via the N3 and O2′ atoms exhibit greater stability than $[dAdo+Na]^+$ binding via the N3 and O3′ atoms. The bidentate $N1NH_2$ and $N7NH_2$ binding modes are also observed for both complexes, and the Gibbs free energies of these conformers increase significantly compared with the ground conformers. In general, $N7NH_2$ binding is more favorable than $N1NH_2$ binding. The 2′-hydroxyl substituent of the $[Ado+Na]^+$ conformers also stabilizes these $N1NH_2$ and $N7NH_2$ conformers vs the analogous conformers of $[dAdo+Na]^+$. Highly compact conformers, such as B1(N7O5′), B1(N3O5′), T1($N7NH_2$O5′), T2($N7NH_2$O5′), and T3($N7NH_2$O5′) of $[dAdo+Na]^+$ and B1(N7O5′) of $[Ado+Na]^+$, are computed to be high Gibbs free energy conformers. Due to the compact nature of these conformers, the hydrogen bonding interaction between the 2′- and 3′-hydroxyl substituents in B1(N7O5′) destabilizes the RNA form complex compared to the corresponding DNA form complex. The relatively high Gibbs free energies of these bidentate conformers again demonstrate that the additional chelation interaction with N3 or O5′ provides important stabilization to these complexes.

DISCUSSION

Conformers of $[dAdo+Na]^+$ Populated by ESI. The measured IRMPD spectrum and calculated IR spectra of the two low-energy conformers of $[dAdo+Na]^+$ that provide the best matches to the measured spectrum are compared in Figure 5. Analogous comparisons to other representative low-energy conformers of $[dAdo+Na]^+$ that exhibit significant mismatches (shaded in red) and thus are not important contributors in the experiments are shown in Figure S4. Overall, the IR spectrum predicted for the ground T1(N3O4′O5′) conformer exhibits the best agreement with the measured IRMPD spectrum in both the FELIX and OPO regions. The interaction between the sodium cation and the N3, O4′, and O5′ atoms forming stable 5- and 6-membered chelation rings to the nucleobase and sugar moieties provides maximum stability to the complex. T2(N3O4′O5′), which differs from the ground conformer by rotations of the 3′-hydroxyl substituent, sugar puckering, and glycosidic bond, which is 1.4 kJ/mol less stable, also exhibits a good agreement with the measured IRMPD spectrum. The primary difference between the calculated IR spectra of T1(N3O4′O5′) and T2(N3O4′O5′) is the width of the peak at 3659 cm^{-1}, which is quite narrow for T1(N3O4′O5′), and a much broader peak for T2(N3O4′O5′). The sharpness of the corresponding feature in the measured IRMPD spectrum suggests that T1(N3O4′O5′) is the major contributor, and that T2(N3O4′O5′) is only present in low abundance in the experiments.

Sodium cation binding to the N3 and O3′ atoms rotates the adenine residue to an *anti* orientation in B1(N3O3′), and increases the relative Gibbs free energy significantly. The absence of the IR band at 930 cm^{-1} and the split of the IR feature at 3659 cm^{-1} (see Figure S4) indicate that B1(N3O3′)

DOI: 10.1021/acs.jpcb.6b06105
J. Phys. Chem. B 2016, 120, 8892−8904

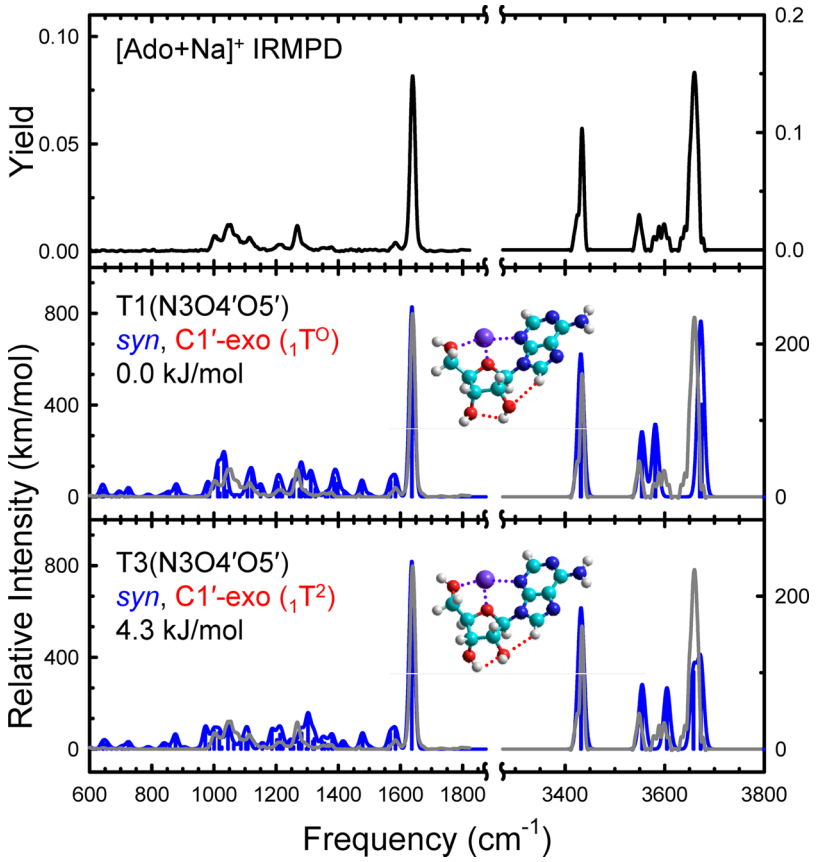

Figure 6. Comparison of the experimental IRMPD action spectrum of $[Ado+Na]^+$ with the B3LYP/6-311+G(d,p) optimized structures and calculated linear IR spectra for the two low-energy conformers of $[Ado+Na]^+$ that best match the measured spectrum. The adenine orientation, sugar configuration, and B3LYP/6-311+G(2d,2p) relative Gibbs free energies at 298 K are also shown.

is not present in measurable abundance in the experiments. As a result of the absence of additional chelation interactions with the sugar moiety, the monodentate conformer, M1(N3), exhibits different sugar puckering and nucleobase orientation and is significantly less stable (>95 kJ/mol). Therefore, the IR spectrum predicted for M1(N3) exhibits distinct shifts in the low frequency region, and a split of the IR band at 3659 cm^{-1}. The IR features predicted in the OPO region for the B1($N7NH_2$) and B1($N1NH_2$) conformers exhibit obvious disagreement with the experimental IRMPD spectrum due to the binding interaction between the sodium cation and the amino substituent of adenine. The Na^+—NH_2 interaction leads to significant variation in the IR features at 1636 and 1583 cm^{-1}, respectively. N1 and N7 binding conformers are significantly less stable, which suggests that they are unlikely to be accessed in the experiments. For B1(O4′O5′), sodium cation binding solely to the sugar moiety increases the relative Gibbs free energy by 41.4 kJ/mol. The additional peak at 960 cm^{-1} and the blue-shifted IR feature at 3690 cm^{-1} in the calculated IR spectrum indicate that B1(O4′O5′) is not present in measurable abundance in the experiments.

In summary, the IR spectrum of the ground T1(N3O4′O5′) conformer exhibits very good agreement with the measured IRMPD spectrum. Therefore, we can conclude that the sodium cation prefers N3 binding to adenine and chelates with the O4′ and O5′ atoms of the sugar moiety, as indicated by the computed relative stabilities of the stable conformers. Furthermore, other tridentate N3 binding conformers with a *syn* orientation of adenine exhibit only minor shifts in the FELIX region, and the broadening at the base of the feature at 3659 cm^{-1} indicates that these conformers are present but in low abundance in the experiments. Because no evidence for peak splitting at 3659 cm^{-1} is observed in the measured spectrum, B1(N3O3′) and M1(N3) do not have measurable populations in the experiments. Due to the huge shifts at 1636 cm^{-1} and the absence of the IR feature at 3433 cm^{-1}, all N1 and N7 binding conformers are unlikely accessed in the experiments. B1(O4′O5′), in which the sodium cation binds to the sugar moiety, exhibits significant shifts and broadening in the calculated IR spectrum, indicating that this conformer also does not have a measurable abundance in the experiments.

Conformers of $[Ado+Na]^+$ Populated by ESI. The measured IRMPD and calculated IR spectra of the two low-energy conformers of $[Ado+Na]^+$ that provide the best matches to the measured spectrum are compared in Figure 6. Analogous comparisons to other representative low-energy conformers of $[Ado+Na]^+$ that exhibit significant mismatches (shaded in red) and thus are not important contributors in the experiments are shown in Figure S5. The T1(N3O4′O5′), T2(N3O4′O5′), and T3(N3O4′O5′) conformers show very good agreement with the measured IRMPD spectrum in the FELIX and OPO regions. However, because the calculated IR spectrum of T2(N3O4′O5′) is virtually identical to that of T1(N3O4′O5′), it is not shown in Figure 6. The shape/broadening at the base of the IRMPD features observed at 3599 and 3659 cm^{-1} suggests that both conformers are present in the experiments. However, theory does not do a good job of predicting the frequency of the IR feature associated with the O5′H stretch, as

DOI: 10.1021/acs.jpcb.6b06105
J. Phys. Chem. B 2016, 120, 8892−8904

there is a blue shift of this feature in all of the computed IR spectra. Therefore, T1(N3O4′O5′) again appears to be the dominant conformer populated in the experiments based on the peak width of the feature near 3659 cm^{-1}. N3 binding conformers exhibiting an *anti* orientation of adenine, B1(N3O2′) and T1(N3O2′O3′), do not have a measurable population in the experiments, due to the significant mismatches observed in the OPO region and high relative Gibbs free energies. The absence of a chelation interaction with O5′ makes B1(N3O4′) 39.5 kJ/mol less stable than the ground conformer, and the IR band predicted at 960 cm^{-1} is not observed in the measured IRMPD spectrum. The N7 or N1 binding modes are less favorable due to the relatively high Gibbs free energy compared with the ground conformer. As found for $[dAdo+Na]^+$, the IR features predicted in the OPO region for B1(N7NH_2) and B1(N1NH_2) exhibit obvious disagreement with the measured IRMPD action spectrum, which is due to the chelation between the sodium cation and the NH_2 substituent. Both the relative Gibbs free energies and the shifts in the IR features of the N1 or N7 binding conformers suggest that the sodium cation prefers to bind to N3 rather than N1 or N7 of adenine. For the bidentate conformer, B1(O4′O5′), the lack of a chelation interaction between Na^+ and adenine makes this conformer 50.5 kJ/mol less stable than the ground conformer. Additionally, poor agreement of the calculated IR spectrum of B1(O4′O5′) also indicates that this bidentate conformer cannot be present in significant abundance in the experiments.

In summary, on the basis of comparisons between the measured IRMPD and calculated IR spectra of $[Ado+Na]^+$ in FELIX and OPO regions, it can be concluded that N1 or N7 binding conformers are unlikely to be populated in the experiments in high abundance. Good agreement is achieved for tridentate complexes that bind via N3, O4′, and O5′, and in particular, for the T1(N3O4′O5′), T2(N3O4′O5′), and T3(N3O4′O5′) conformers with puckering of the sugar moiety that is approximately C1′-exo, but lies between C2′-endo and O4′-endo, and a *syn* orientation of adenine indicating that these conformers are present in the experiments. T1(N3O4′O5′) and T2(N3O4′O5′) are likely present at higher populations than T3(N3O4′O5′) as a result of their greater similarity regarding the feature observed at 3659 cm^{-1}. The *anti* orientated N3 binding conformers, B1(N3O2′) and T1(N3O2′O3′), do not have measurable populations in the experiments due to the significant differences between the computed and measured spectra in the OPO region. Both high Gibbs free energy and mismatch of the calculated IR spectrum suggest that B1(N3O4′) has very low abundance in the experiments.

Vibrational Assignments for $[dAdo+Na]^+$ and $[Ado+Na]^+$. The vibrational assignments for the ground conformers of $[dAdo+Na]^+$ and $[Ado+Na]^+$ are shown in Table 3 and based on the T1(N3O4′O5′) conformers of these species. The measured IRMPD spectra of $[dAdo+Na]^+$ and $[Ado+Na]^+$ are highly parallel, and only small shifts (<10 cm^{-1}) are observed for each vibrational mode. Two notable differences in the IRMPD spectra of $[dAdo+Na]^+$ and $[Ado+Na]^+$ are, however, observed. In the FELIX region, the IRMPD feature associated with C2′−C3′ stretching at 930 cm^{-1} is only observed for $[dAdo+Na]^+$. In the OPO region, the weak IR feature at ∼3600 cm^{-1} reflects the 2′-hydroxyl stretch, which is obviously only observed for $[Ado+Na]^+$. As summarized in the table, the features below 1550 cm^{-1} and above 3550 cm^{-1} are associated with the sugar moiety, whereas those between these limits arise from the nucleobase. Both spectral regions are important to the assignment of the structures populated in the experiments. In general, the gross structural features of these complexes (i.e., the mode of cation binding and nucleobase orientation) are readily deduced from the IR signatures observed in either the FELIX or OPO region. However, both spectral regions are important for elucidating minor structural differences and for definitively establishing the dominant conformers populated in the experiments.

Table 3. Vibrational Assignments for the Ground-State Conformers of $[dAdo+Na]^+$ and $[Ado+Na]^+$ [a]

vibrational mode	$[dAdo+Na]^+$	$[Ado+Na]^+$
C2′−C3′ stretching	930	N/A
sugar ring stretching	960 to 1150	976 to 1146
sugar hydrogen bending	1269	1269
nucleobase ring stretching	1583	1590
NH_2 scissoring and C−NH_2 stretching	1636	1640
NH_2 symmetric stretching	3433	3433
NH_2 asymmetric stretching	3551	3549
2′-hydroxyl stretching	N/A	3599
3′- and 5′-hydroxyl stretching	3659	3659

[a]All values are given in cm^{-1}.

Influence of Sodium Cationization vs Protonation on the IRMPD Spectra of dAdo and Ado. IRMPD action spectroscopy and theoretical studies of the gas-phase conformations and energetics of $[dAdo+H]^+$ and $[Ado+H]^+$ have previously been reported by our group.[6] The IRMPD yields observed for the protonated systems are much larger than those of the analogous Na^+ complexes. The much lower IRMPD yields for the sodium complexes arise because more energy is required to induce dissociation, and thus indicate that the sodium cation is much less effective at activating the glycosidic bond. In the FELIX region, the IRMPD features of $[dAdo+Na]^+$ and $[Ado+Na]^+$ associated with the nucleobase (those above ∼1300 cm^{-1}) exhibit similar peak shapes but appear at frequencies ∼30 cm^{-1} below the analogous features observed for $[dAdo+H]^+$ and $[Ado+H]^+$ (see Figure 2). These red shifts are consistent with the stronger binding of a proton than sodium cation, thus leading to greater withdrawal of electron density from the adenine moiety. In contrast, the IRMPD features associated with the sugar moiety (those below ∼1300 cm^{-1}) of the protonated versus sodium cationized nucleosides show striking differences, particular in the C−O stretching region, which are likely due to the change in sugar puckering induced by the involvement of the O4′ atom of the sugar in the binding of the sodium cation. In the OPO region, the peak shapes of these ions are correspondingly similar. However, compared to $[dAdo+H]^+$ and $[Ado+H]^+$, the IR absorption at ∼3660 cm^{-1} shifts to the red by ∼5 cm^{-1}, whereas all of the IR absorptions below ∼3640 cm^{-1} exhibit blue shifts of 10−20 cm^{-1}. These blue shifts are again consistent with the ability of a proton to withdraw more electron density than a sodium cation from the adenine moiety, and in particular, the amino nitrogen atom, thereby strengthening the N−H bonds.

Comparison of the Low-Energy Conformers of $[dAdo+Na]^+$, $[Ado+Na]^+$, $[dAdo+H]^+$, and $[Ado+H]^+$. Our previous IRMPD action spectroscopy and theoretical study of the gas-phase conformations and energetics of $[dAdo+H]^+$ and $[Ado+H]^+$ [6] found N3 to be the most favorable protonation site for both $[dAdo+H]^+$ and $[Ado+H]^+$. (The ground-state

DOI: 10.1021/acs.jpcb.6b06105
J. Phys. Chem. B 2016, 120, 8892−8904

structures of $[dAdo+H]^+$ and $[Ado+H]^+$ are shown in Figure 1 for comparison.) N3 protonation enables a strong intramolecular hydrogen-bonding interaction between $N3H^+$ and O5′ to be formed, leading to rotation of adenine to a *syn* orientation and an approximately C2′-endo ($^2T_1$) configuration of the sugar. In contrast, protonation at N1 and N7 is found to be much less favorable such that N1 protonated conformers are observed in minor abundance and N7 conformers are not present in measurable abundance, consistent with the computed stabilities which follow the order N3 > N1 > N7. For $[dAdo+H]^+$, the N1 binding conformers are at least 25.3 kJ/mol less stable and the N7 binding conformers are at least 33.6 kJ/mol less stable than the ground conformer. For $[Ado+H]^+$, the relative Gibbs free energies of N1 binding conformers reduce to at least 21.8 kJ/mol, whereas the relative Gibbs free energies of N7 binding conformers increase to at least 37.2 kJ/mol. Similarly, the sodium cation prefers to bind to the N3, O4′, and O5′ atoms and also requires that adenine rotate to a *syn* orientation. However, because the sodium cation is much larger and can form multiple chelating interactions, the O4′ atom is also involved in the binding of Na^+, and thus forms 5- and 6-membered rings in the ground conformers of $[dAdo+Na]^+$ and $[Ado+Na]^+$. Interaction of the sodium cation with the O4′ atom influences the sugar puckering, which shifts from C2′-endo (^2E) in the protonated systems toward O4′-endo (^OE) in the sodium cationized systems, with multiple low-energy conformers exhibiting puckering of the sugar moiety that lie between these limiting configurations. Sodium cation binding to the N1 or N7 atoms is much less favorable and not observed in the experiments. For $[dAdo+Na]^+$, the N7 binding conformers are at least 65.0 kJ/mol less stable, whereas the N1 binding conformers are at least 73.1 kJ/mol less stable than the ground conformer. For $[Ado+Na]^+$, the relative Gibbs free energies of the N7 and N1 binding conformers are similar to those found for $[dAdo+Na]^+$ but are slightly more favorable such that the most stable N7 binding conformer is 60.3 kJ/mol, whereas the most stable N1 binding conformer is 67.1 kJ/mol less favorable than the ground conformer. The binding affinities follow the order N3 > N7 > N1. Thus, the sodium cation alters the relative affinities for N1 and N7 binding compared to a proton. Additionally, the N1 and N7 binding conformers of $[dAdo+Na]^+$ and $[Ado+Na]^+$ are much less stable than the corresponding ground conformers. The glycosidic bonds of the sodium cationized adenine nucleosides are shorter than those of the protonated species (1.458 Å in $[dAdo+Na]^+$ and 1.448 Å in $[Ado+Na]^+$ vs 1.465 Å in $[dAdo+H]^+$ and 1.459 Å in $[Ado+H]^+$), indicating that sodium cationization is less effective at activating the glycosidic bond than protonation.

Relative N-Glycosidic Bond Stabilities of Protonated and Sodium Cationized dAdo and Ado. Figure 4 compares the survival yield analyses of $[dAdo+H]^+$, $[Ado+H]^+$, and $[dAdo+Na]^+$. Because the only fragmentation pathway observed for $[dAdo+H]^+$, $[Ado+H]^+$, and $[dAdo+Na]^+$ involves N-glycosidic bond cleavage, the trends in the $CID_{50\%}$ values provide a direct measure of the relative N-glycosidic bond stabilities. The $CID_{50\%}$ value of $[Ado+H]^+$ exceeds that of $[dAdo+H]^+$, which suggests that the 2′-hydroxyl substituent of Ado stabilizes the N-glycosidic bond. This result is consistent with TCID results recently reported for these adenine nucleosides, where the activation energies at 0 K for N-glycosidic bond cleavage of N3 protonated $[dAdo+H]^+$ and $[Ado+H]^+$ were measured as 147.6 ± 4.8 and 164.0 ± 4.8 kJ/mol, respectively.[62] Analogous behavior has also been found in TCID studies of the protonated guanine and cytosine nucleosides,[63,64] suggesting that in general RNA glycosidic bonds are more stable than the analogous DNA glycosidic bonds. These trends are also consistent with the computed C1−N9 glycosidic bond lengths discussed in the previous section. The same conclusion can be drawn by comparing the fragmentation behavior of $[dAdo+Na]^+$ and $[Ado+Na]^+$. The only CID fragmentation pathway of $[Ado+Na]^+$ is the loss of neutral adenosine, which is empirical evidence that suggests that the N-glycosidic bond of $[Ado+Na]^+$ is more stable than that of $[dAdo+Na]^+$. In summary, the N-glycosidic bond of dAdo is less stable than that of Ado for both the protonated and sodium cationized species. In addition, the N-glycosidic bonds of sodium cationized dAdo and Ado are more stable than those of protonated dAdo and Ado, respectively. Thus, sodium cationization activates the N-glycosidic bond less effectively than protonation.

Influence of the Sugar Moiety on the Binding of Na^+ to Adenine. Sodium cation binding to adenine was studied via *ab initio* calculations and TCID experiments.[70,71] In the case of the canonical N9−H tautomer, the most favorable binding mode of a sodium cation involves chelation to N7 and NH_2, forming a 5-membered ring. Considering all possible adenine tautomers, the lowest-energy structure for a sodium cationized adenine complex has been found to be the minor N7−H adenine tautomer with the sodium cation binding to the N3 and N9 atoms.[70,72] For the sodium cationized DNA and RNA nucleosides, the presence of the sugar moiety blocks the N9 atom of adenine such that the preferred binding mode must necessarily differ. Binding to N3 of adenine, with additional chelation interactions with the O4′ and O5′ atoms of the sugar moiety, leads to the formation of 5- and 6-membered chelation rings. These chelation interactions provide additional stabilization to the complexes, which makes the N3 position of adenine much more favorable than the N7 and NH_2 chelation mode.

CONCLUSIONS

Comparisons between the measured IRMPD and calculated IR spectra of the $[dAdo+Na]^+$ and $[Ado+Na]^+$ complexes find that the only conformers populated by ESI for both of these systems involve the sodium cation binding to the N3, O4′, and O5′ atoms. Such tridentate binding leads to the formation of 5- and 6-membered chelation rings with adenine in a *syn* orientation, and puckering of the sugar moiety that lies between C2′-endo and O4′-endo. The presence of multiple conformers differing primarily in the rotation of 2′- and 3′-hydroxyl substituents of $[Ado+Na]^+$ leads to broadening at the base of the IR feature at 3659 cm^{-1}, indicating the presence of these excited rotamers in the experiments. Conformers lacking one of the chelation interactions between the sodium cation and the nucleoside are significantly destabilized and lead to large spectral shifts in the OPO region that do not appear in the measured IRMPD spectra of $[dAdo+Na]^+$ and $[Ado+Na]^+$. Conformers involving sodium cation binding to the N1 or N7 atoms also chelate with the NH_2 substituent, which produces shifts in the calculated IR features for the C−NH_2 stretching in the FELIX region and symmetric and asymmetric NH_2 stretching in the OPO region that are not experimentally observed. These differences suggest that N1 and N7 binding conformers of $[dAdo+Na]^+$ and $[Ado+Na]^+$ are not present in measurable abundance in the experiments. The only fragmentation pathway observed in the ER-CID experiments for $[dAdo+H]^+$, $[Ado+H]^+$, and $[dAdo+Na]^+$ involves N-glycosidic bond cleavage. In contrast,

DOI: 10.1021/acs.jpcb.6b06105
J. Phys. Chem. B 2016, 120, 8892−8904

the only CID fragmentation pathway that occurs for $[Ado+Na]^+$ presumably involves loss of neutral adenosine, as no products are detected due to the low mass cutoff for CID in the QIT MS. Survival yield analyses of $[dAdo+H]^+$, $[Ado+H]^+$, and $[dAdo+Na]^+$ are compared to elucidate the relative N-glycosidic bond stabilities. Trends in the ER-CID behavior and $CID_{50\%}$ values for these systems suggest that the 2′-hydroxyl substituent in the RNA nucleoside stabilizes the N-glycosidic bond, and that sodium cationization of dAdo and Ado activates the N-glycosidic bond less effectively than protonation. These energy-resolved CID results exhibit good agreement with the IRMPD yields of $[dAdo+Na]^+$ and $[Ado+Na]^+$, and the computed N-glycosidic bond lengths.

■ ASSOCIATED CONTENT

Supporting Information

The Supporting Information is available free of charge on the ACS Publications website at DOI: 10.1021/acs.jpcb.6b06105.

Complete citation for ref 61. Figures and a table summarizing the structures of all low-energy conformers of $[dAdo+Na]^+$ and $[Ado+Na]^+$ computed within 100 kJ/mol of the ground conformers along with the conformer designations, modes of sodium cation binding, orientations of adenine, sugar puckering, and relative Gibbs free energies at 298 K (PDF)

■ AUTHOR INFORMATION

Corresponding Author

*E-mail: mrodgers@chem.wayne.edu. Phone: (313)577-2431.

Notes

The authors declare no competing financial interest.

■ ACKNOWLEDGMENTS

This work was financially supported by the National Science Foundation, Grants OISE-0730072 and OISE-1357787 (for the IRMPD measurements), DBI-0922819 (for the Bruker amaZon ETD QIT MS used in this work), and CHE-1409420 (for the calculations and other research costs). Y.Z. gratefully acknowledges support from a Wayne State University Thomas C. Rumble Graduate Fellowship. S.F.S. and J.K.L. acknowledge support as REUs of the MS-PIRE and MS-IRES programs, respectively. We also thank Wayne State University C&IT for computational resources and support. This work is part of the research program of FOM, which is financially supported by the Nederlandse Organisatie voor Wetenschappelijk Onderzoek (NWO). The skillful assistance of the FELIX staff is gratefully acknowledged.

■ REFERENCES

(1) van Dam, L.; Ouwerkerk, N.; Brinkmann, A.; Raap, J.; Levitt, M. H. Solid-State NMR Determination of Sugar Ring Pucker in C-13-Labeled 2′-Deoxynucleosides. *Biophys. J.* **2002**, *83*, 2835−2844.

(2) Rich, A.; Nordheim, A.; Wang, A. H. J. The Chemistry and Biology of Left-Handed Z-DNA. *Annu. Rev. Biochem.* **1984**, *53*, 791−846.

(3) Saenger, W. *Principles of Nucleic-Acid Structure* Cantor, C. R., Ed.; Springer-Verlag: New York, 1984; pp 16−104.

(4) Lippard, S. J.; Berg, J. M. *Principles of Bioinorganic Chemistry*; University Science Books: Mill Valley, CA, 1994; pp 57−69.

(5) Wu, R. R.; Yang, B.; Berden, G.; Oomens, J.; Rodgers, M. T. Gas-Phase Conformations and Energetics of Protonated 2′-Deoxyguanosine and Guanosine: IRMPD Action Spectroscopy and Theoretical Studies. *J. Phys. Chem. B* **2014**, *118*, 14774−14784.

(6) Wu, R. R.; Yang, B.; Berden, G.; Oomens, J.; Rodgers, M. T. Gas-Phase Conformations and Energetics of Protonated 2′-Deoxyadenosine and Adenosine: IRMPD Action Spectroscopy and Theoretical Studies. *J. Phys. Chem. B* **2015**, *119*, 2795−2805.

(7) Wu, R. R.; Yang, B.; Frieler, C. E.; Berden, G.; Oomens, J.; Rodgers, M. T. Diverse Mixtures of 2,4-Dihydroxy Tautomers and O4 Protonated Conformers of Uridine and 2′-Deoxyuridine Coexist in the Gas Phase. *Phys. Chem. Chem. Phys.* **2015**, *17*, 25978−25988.

(8) Wu, R. R.; Yang, B.; Frieler, C. E.; Berden, G.; Oomens, J.; Rodgers, M. T. N3 and O2 Protonated Tautomeric Conformations of 2′-Deoxycytidine and Cytidine Coexist in the Gas Phase. *J. Phys. Chem. B* **2015**, *119*, 5773−5784.

(9) Wu, R. R.; Yang, B.; Frieler, C. E.; Berden, G.; Oomens, J.; Rodgers, M. T. 2,4-Dihydroxy and O2 Protonated Tautomers of dThd and Thd Coexist in the Gas Phase: Methylation Alters Protonation Preferences versus dUrd and Urd. *J. Am. Soc. Mass Spectrom.* **2016**, *27*, 410−421.

(10) Altona, C.; Sundaral, M. Conformational-Analysis of Sugar Ring in Nucleosides and Nucleotides - New Description Using Concept of Pseudorotation. *J. Am. Chem. Soc.* **1972**, *94*, 8205−8212.

(11) Obika, S.; Nanbu, D.; Hari, Y.; Andoh, J.; Morio, K.; Doi, T.; Imanishi, T. Stability and Structural Features of the Duplexes Containing Nucleoside Analogues with a Fixed N-Type Conformation, 2′-O,4′-C-Methyleneribonucleosides. *Tetrahedron Lett.* **1998**, *39*, 5401−5404.

(12) Haschemeyer, A. E. V.; Rich, A. Nucleoside Confromations - An Analysis of Steric Barriers to Rotation About the Gylcosidic Bond. *J. Mol. Biol.* **1967**, *27*, 369−384.

(13) Eichhorn, G. L. Conformational Change Induced by Metal-Ions Through Coordination. *Coord. Chem. Rev.* **1993**, *128*, 167−173.

(14) Baldwin, S. A.; Mackay, J. R.; Cass, C. E.; Young, J. D. Nucleoside Transporters: Molecular Biology and Implications for Therapeutic Development. *Mol. Med. Today* **1999**, *5*, 216−224.

(15) Ritzel, M. W. L.; Yao, S. Y. M.; Huang, M. Y.; Elliott, J. F.; Cass, C. E.; Young, J. D. Molecular Cloning and Functional Expression of cDNAs Encoding a Human Na^+-Nucleoside Cotransporter (hCNT1). *Am. J. Physiol.: Cell Physiol.* **1997**, *272*, C707−C714.

(16) Yao, S. Y. M.; Ng, A. M. L.; Ritzel, M. W. L.; Gati, W. P.; Cass, C. E.; Young, J. D. Transport of Adenosine by Recombinant Purine- and Pyrimidine-Selective Sodium/Nucleoside Cotransporters from Rat Jejunum Expressed in Xenopus Laevis Oocytes. *Mol. Pharmacol.* **1996**, *50*, 1529−1535.

(17) Vickers, M. F.; Young, J. D.; Baldwin, S. A.; Ellison, M. J.; Cass, C. E. Functional Production of Mammalian Concentrative Nucleoside Transporters in Saccharomyces Cerevisiae. *Mol. Membr. Biol.* **2001**, *18*, 73−79.

(18) Wang, J.; Su, S. F.; Dresser, M. J.; Schaner, M. E.; Washington, C. B.; Giacomini, K. M. Na(+)-Dependent Purine Nucleoside Transporter from Human Kidney: Cloning and Functional Characterization. *Am. J. Physiol.: Renal, Fluid Electrolyte Physiol.* **1997**, *273*, F1058−F1065.

(19) Rlteel, M. W. L.; Yaof, S. Y. M.; Ng, A. M. L.; Mackeyt, J. R.; Cass, C. E.; Young, J. D. Molecular Cloning, Functional Expression and Chromosomal Localization of a cDNA Encoding a Human Na^+/Nucleoside Cotransporter (hCNT2) Selective for Purine Nucleosides and Uridine. *Mol. Membr. Biol.* **1998**, *15*, 203−211.

(20) Hamilton, S. R.; Yao, S. Y. M.; Ingram, J. C.; Hadden, D. A.; Ritzel, M. W. L.; Gallagher, M. P.; Henderson, P. J. F.; Cass, C. E.; Young, J. D.; Baldwin, S. A. Subcellular Distribution and Membrane Topology of the Mammalian Concentrative Na^+-Nucleoside Cotransporter rCNT1. *J. Biol. Chem.* **2001**, *276*, 27981−27988.

(21) Yao, S. Y.; Ng, A. M.; Loewen, S. K.; Cass, C. E.; Baldwin, S. A.; Young, J. D. An Ancient Prevertebrate Na^+-Nucleoside Cotransporter (hfCNT) from the Pacific Hagfish (Eptatretus stouti). *Am. J. Physiol.-Cell. Ph.* **2002**, *283*, C155−C168.

(22) Smith, K. M.; Ng, A. M. L.; Yao, S. Y. M.; Labedz, K. A.; Knaus, E. E.; Wiebe, L. I.; Cass, C. E.; Baldwin, S. A.; Chen, X. Z.; Karpinski, E.; Young, J. D. Electrophysiological Characterization of a Recombi-

DOI: 10.1021/acs.jpcb.6b06105
J. Phys. Chem. B 2016, 120, 8892−8904

nant Human Na^+-Coupled Nucleoside Transporter (hCNT1) Produced in Xenopus Oocytes. *J. Physiol.* **2004**, *558*, 807−823.
(23) Smith, K. M.; Slugoski, M. D.; Loewen, S. K.; Ng, A. M. L.; Yao, S. Y. M.; Chen, X. Z.; Karpinski, E.; Cass, C. E.; Baldwin, S. A.; Young, J. D. The Broadly Selective Human Na(+)/Nucleoside Cotransporter (hCNT3) Exhibits Novel Cation-Coupled Nucleoside Transport Characteristics. *J. Biol. Chem.* **2005**, *280*, 25436−25449.
(24) Ritzel, M. W. L.; Ng, A. M. L.; Yao, S. Y. M.; Graham, K.; Loewen, S. K.; Smith, K. M.; Hyde, R. J.; Karpinski, E.; Cass, C. E.; Baldwin, S. A.; Young, J. D. Recent Molecular Advances in Studies of the Concentrative Na^+-Dependent Nucleoside Transporter (CNT) Family: Identification and Characterization of Novel Human and Mouse Proteins (hCNT3 and mCNT3) Broadly Selective for Purine and Pyrimidine Nucleosides (System cib). *Mol. Membr. Biol.* **2001**, *18*, 65−72.
(25) Ritzel, M. W. L.; Ng, A. M. L.; Yao, S. Y. M.; Graham, K.; Loewen, S. K.; Smith, K. N.; Ritzel, R. G.; Mowles, D. A.; Carpenter, P.; Chen, X. Z.; Karpinski, E.; Hyde, R. J.; Baldwin, S. A.; Cass, C. E.; Young, J. D. Molecular Identification and Characterization of Novel Human and Mouse Concentrative Na^+-Nucleoside Cotransporter Proteins (hCNT3 and mCNT3) Broadly Selective for Purine and Pyrimidine Nucleosides (System cib). *J. Biol. Chem.* **2001**, *276*, 2914−2927.
(26) Giblett, E. R.; Anderson, J. E.; Cohen, F.; Pollara, B.; Meuwissen, H. J. Adenosine-Deaminase Deficiency in Two Patients with Severely Impaired Cellular Immunity. *J. Immunol.* **2012**, *188*, 936−938.
(27) Martin, D. W.; Gelfand, E. W. Biochemistry of Diseases of Immunodevelopment. *Annu. Rev. Biochem.* **1981**, *50*, 845−877.
(28) Seto, S.; Carrera, C. J.; Kubota, M.; Wasson, D. B.; Carson, D. A. Mechanism of Deoxyadenosine and 2-Chlorodeoxyadenosine Toxicity to Nondividing Human-Lymphocytes. *J. Clin. Invest.* **1985**, *75*, 377−383.
(29) Mitchell, B. S.; Mejias, E.; Daddona, P. E.; Kelley, W. N. Purinogenic Immunodeficiency Diseases-Selective Toxicity of Deoxyribonucleosides for T-Cells. *Proc. Natl. Acad. Sci. U. S. A.* **1978**, *75*, 5011−5014.
(30) Ohmori, M.; Ohmori, K.; Hasunuma, K. Rapid Change in Cyclic 3′,5′-AMP Concentration Triggered by a Light-Off or Light-on Signal in Anabaena-Cylindrica. *Arch. Microbiol.* **1988**, *150*, 203−204.
(31) Moutinho, A.; Hussey, P. J.; Trewavas, A. J.; Malho, R. cAMP Acts as a Second Messenger in Pollen Tube Growth and Reorientation. *Proc. Natl. Acad. Sci. U. S. A.* **2001**, *98*, 10481−10486.
(32) Eltzschig, H. K.; Carmeliet, P. Mechanisms of Disease: Hypoxia and Inflammation. *N. Engl. J. Med.* **2011**, *364*, 656−665.
(33) Eltzschig, H. K.; Sitkovsky, M. V.; Robson, S. C. Mechanisms of Disease Purinergic Signaling During Inflammation. *N. Engl. J. Med.* **2012**, *367*, 2322−2333.
(34) Eltzschig, H. K. Extracellular Adenosine Signaling in Molecular Medicine. *J. Mol. Med.* **2013**, *91*, 141−146.
(35) Jackson, E. K.; Raghvendra, D. K. The Extracellular Cyclic AMP-Adenosine Pathway in Renal Physiology. *Annu. Rev. Physiol.* **2004**, *66*, 571−599.
(36) Jackson, E. K. The 2′,3′-cAMP-Adenosine Pathway. *Am. J. Physiol.-Renal.* **2011**, *301*, F1160−F1167.
(37) Jackson, E. K.; Cheng, D. M.; Jackson, T. C.; Verrier, J. D.; Gillespie, D. G. Extracellular Guanosine Regulates Extracellular Adenosine Levels. *Am. J. Physiol-Cell Ph.* **2013**, *304*, C406−C421.
(38) Nei, Y.-w.; Akinyemi, T. E.; Kaczan, C. M.; Steill, J. D.; Berden, G.; Oomens, J.; Rodgers, M. T. Infrared Multiple Photon Dissociation Action Spectroscopy of Sodiated Uracil and Thiouracils: Effects of Thioketo-Substitution on Gas-Phase Conformation. *Int. J. Mass Spectrom.* **2011**, *308*, 191−202.
(39) Nei, Y.-w.; Akinyemi, T. E.; Steill, J. D.; Oomens, J.; Rodgers, M. T. Infrared Multiple Photon Dissociation Action Spectroscopy of Protonated Uracil and Thiouracils: Effects of Thioketo-Substitution on Gas-Phase Conformation. *Int. J. Mass Spectrom.* **2010**, *297*, 139−151.
(40) Crampton, K. T.; Rathur, A. I.; Nei, Y.-w.; Berden, G.; Oomens, J.; Rodgers, M. T. Protonation Preferentially Stabilizes Minor Tautomers of the Halouracils: IRMPD Action Spectroscopy and Theoretical Studies. *J. Am. Soc. Mass Spectrom.* **2012**, *23*, 1469−1478.
(41) Kaczan, C. M.; Rathur, A. I.; Wu, R. R.; Chen, Y.; Austin, C. A.; Berden, G.; Oomens, J.; Rodgers, M. T. Infrared Multiple Photon Dissociation Action Spectroscopy of Sodium Cationized Halouracils: Effects of Sodium Cationization and Halogenation on Gas-Phase Conformation. *Int. J. Mass Spectrom.* **2015**, *378*, 76−85.
(42) Oomens, J.; Moehlig, A. R.; Morton, T. H. Infrared Multiple Photon Dissociation (IRMPD) Spectroscopy of the Proton-Bound Dimer of 1-Methylcytosine in the Gas Phase. *J. Phys. Chem. Lett.* **2010**, *1*, 2891−2897.
(43) Salpin, J. Y.; Haldys, V.; Guillaumont, S.; Tortajada, J.; Hurtado, M.; Lamsabhi, A. Gas-Phase Interactions between Lead(II) Ions and Cytosine: Tandem Mass Spectrometry and Infrared Multiple-Photon Dissociation Spectroscopy Study. *ChemPhysChem* **2014**, *15*, 2959−2971.
(44) Yang, B.; Wu, R. R.; Berden, G.; Oomens, J.; Rodgers, M. T. Infrared Multiple Photon Dissociation Action Spectroscopy of Proton-Bound Dimers of Cytosine and Modified Cytosines: Effects of Modifications on Gas-Phase Conformations. *J. Phys. Chem. B* **2013**, *117*, 14191−14201.
(45) Yang, B.; Wu, R. R.; Polfer, N. C.; Berden, G.; Oomens, J.; Rodgers, M. T. IRMPD Action Spectroscopy of Alkali Metal Cation-Cytosine Complexes: Effects of Alkali Metal Cation Size on Gas Phase Conformation. *J. Am. Soc. Mass Spectrom.* **2013**, *24*, 1523−1533.
(46) Ung, H. U.; Huynh, K. T.; Poutsma, J. C.; Oomens, J.; Berden, G.; Morton, T. H. Investigation of Proton Affinities and Gas Phase Vibrational Spectra of Protonated Nucleosides, Deoxynucleosides, and Their Analogs. *Int. J. Mass Spectrom.* **2015**, *378*, 294−302.
(47) Filippi, A.; Fraschetti, C.; Rondino, F.; Piccirillo, S.; Steinmetz, V.; Guidoni, L.; Speranza, M. Protonated Pyrimidine Nucleosides Probed by IRMPD Spectroscopy. *Int. J. Mass Spectrom.* **2013**, *354*−*355*, 54−61.
(48) Nei, Y. W.; Hallowita, N.; Steill, J. D.; Oomens, J.; Rodgers, M. T. Infrared Multiple Photon Dissociation Action Spectroscopy of Deprotonated DNA Mononucleotides: Gas-Phase Conformations and Energetics. *J. Phys. Chem. A* **2013**, *117*, 1319−1335.
(49) Nei, Y. W.; Crampton, K. T.; Berden, G.; Oomens, J.; Rodgers, M. T. Infrared Multiple Photon Dissociation Action Spectroscopy of Deprotonated RNA Mononucleotides: Gas-Phase Conformations and Energetics. *J. Phys. Chem. A* **2013**, *117*, 10634−10649.
(50) Wu, R. R.; He, C. C.; Hamlow, L. A.; Nei, Y.-w.; Berden, G.; Oomens, J.; Rodgers, M. T. Protonation Induced Base Rotation of Purine Nucleotides pdGuo and pGuo. *Phys. Chem. Chem. Phys.* **2016**, *18*, 15081−15090.
(51) Wu, R. R.; He, C. C.; Hamlow, L. A.; Nei, Y.-w.; Berden, G.; Oomens, J.; Rodgers, M. T. N3 Protonation Induces Base Rotation of 2′-Deoxyadenosine-5′-monophosphate and Adenosine-5′-monophosphate. *J. Phys. Chem. B* **2016**, *120*, 4616−4624.
(52) Chiavarino, B.; Crestoni, M. E.; Fornarini, S.; Lanucara, F.; Lemaire, J.; Maitre, P.; Scuderib, D. Infrared Spectroscopy of Isolated Nucleotides 1. The Cyclic 3′,5′-Adenosine Monophosphate Anion. *Int. J. Mass Spectrom.* **2008**, *270*, 111−117.
(53) Lanucara, F.; Crestoni, M. E.; Chiavarino, B.; Fornarini, S.; Hernandez, O.; Scuderi, D.; Maitre, P. Infrared Spectroscopy of Nucleotides in the Gas Phase 2. The Protonated Cyclic 3′,5′-Adenosine Monophosphate. *RSC Adv.* **2013**, *3*, 12711−12720.
(54) Ligare, M. R.; Rijs, A. M.; Berden, G.; Kabelac, M.; Nachtigallova, D.; Oomens, J.; de Vries, M. S. Resonant Infrared Multiple Photon Dissociation Spectroscopy of Anionic Nucleotide Monophosphate Clusters. *J. Phys. Chem. B* **2015**, *119*, 7894−7901.
(55) Salpin, J. Y.; MacAleese, L.; Chirot, F.; Dugourd, P. Structure of the Pb^{2+}-Deprotonated dGMP Complex in the Gas Phase: A Combined MS-MS/IRMPD Spectroscopy/Ion Mobility Study. *Phys. Chem. Chem. Phys.* **2014**, *16*, 14127−14138.
(56) Oepts, D.; van der Meer, A. F. G.; Vanamersfoort, P. W. The Free-Electron-Laser User Facility FELIX. *Infrared Phys. Technol.* **1995**, *36*, 297−308.

DOI: 10.1021/acs.jpcb.6b06105
J. Phys. Chem. B 2016, 120, 8892−8904

(57) Polfer, N. C.; Oomens, J.; Moore, D. T.; von Helden, G.; Meijer, G.; Dunbar, R. C. Infrared Spectroscopy of Phenylalanine Ag(I) and Zn(II) Complexes in the Gas Phase. *J. Am. Chem. Soc.* **2006**, *128*, 517−525.
(58) Valle, J. J.; Eyler, J. R.; Oomens, J.; Moore, D. T.; van der Meer, A. F. G.; von Helden, G.; Meijer, G.; Hendrickson, C. L.; Marshall, A. G.; Blakney, G. T. Free Electron Laser-Fourier Transform Ion Cyclotron Resonance Mass Spectrometry Facility for Obtaining Infrared Multiphoton Dissociation Spectra of Gaseous Ions. *Rev. Sci. Instrum.* **2005**, *76*, 023103.
(59) Polfer, N. C.; Oomens, J. Reaction Products in Mass Spectrometry Elucidated with Infrared Spectroscopy. *Phys. Chem. Chem. Phys.* **2007**, *9*, 3804−3817.
(60) *HyperChem Computational Chemistry Software Package*, version 5.0; Hypercube, Inc.: Gainsville, FL, 1997.
(61) Frisch, M. J.; Trucks, G. W.; Schlegel, H. B.; Scuseria, G. E.; Robb, M. A.; Cheeseman, J. R.; Scalmani, G.; Barone, V.; Mennucci, B.; Petersson, G. A.; et al. *Gaussian 09*, revision C.01; Gaussian, Inc.: Wallingford, CT, 2009 (see the Supporting Information for the complete citation).
(62) Wu, R. R.; Rodgers, M. T. Mechanisms and Energetics for N-Glycosidic Bond Cleavage of Protonated Adenine Nucleosides: N3 Protonation Induces Base Rotation and Enhances N-Glycosidic Bond Stability. *Phys. Chem. Chem. Phys.* **2016**, *18*, 16021−32.
(63) Wu, R. R.; Rodgers, M. T. O2 Protonation Controls Threshold Behavior for N-Glycosidic Bond Cleavage of Protonated Cytosine Nucleosides. *J. Phys. Chem. B* **2016**, *120*, 4803−4811.
(64) Wu, R. R.; Chen, Y.; Rodgers, M. T. Mechanisms and Energetics for N-Glycosidic Bond Cleavage of Protonated 2′-Deoxyguanosine and Guanosine. *Phys. Chem. Chem. Phys.* **2016**, *18*, 2968−2980.
(65) Memboeuf, A.; Nasioudis, A.; Indelicato, S.; Pollreisz, F.; Kuki, A.; Keki, S.; van den Brink, O. F.; Vekey, K.; Drahos, L. Size Effect on Fragmentation in Tandem Mass Spectrometry. *Anal. Chem.* **2010**, *82*, 2294−2302.
(66) Derwa, F.; Depauw, E.; Natalis, P. New Basis for a Method for the Estimation of Secondary Ion Internal Energy-Distribution in Soft Ionization Techniques. *Org. Mass Spectrom.* **1991**, *26*, 117−118.
(67) Guo, X. H.; Duursma, M. C.; Kistemaker, P. G.; Nibbering, N. M. M.; Vekey, K.; Drahos, L.; Heeren, R. M. A. Manipulating Internal Energy of Protonated Biomolecules in Electrospray Ionization Fourier Transform Ion Cyclotron Resonance Mass Spectrometry. *J. Mass Spectrom.* **2003**, *38*, 597−606.
(68) Memboeuf, A.; Jullien, L.; Lartia, R.; Brasme, B.; Gimbert, Y. Tandem Mass Spectrometric Analysis of a Mixture of Isobars Using the Survival Yield Technique. *J. Am. Soc. Mass Spectrom.* **2011**, *22*, 1744−1752.
(69) Kertesz, T. M.; Hall, L. H.; Hill, D. W.; Grant, D. F. CE50: Quantifying Collision Induced Dissociation Energy for Small Molecule Characterization and Identification. *J. Am. Soc. Mass Spectrom.* **2009**, *20*, 1759−1767.
(70) Kabelac, M.; Hobza, P. Na^+, Mg^{2+}, and Zn^{2+} Binding to All Tautomers of Adenine, Cytosine, and Thymine and the Eight Most Stable Keto/Enol Tautomers of Guanine: A Correlated ab Initio Quantum Chemical Study. *J. Phys. Chem. B* **2006**, *110*, 14515−14523.
(71) Rodgers, M. T.; Armentrout, P. B. Noncovalent Interactions of Nucleic Acid Bases (Uracil, Thymine, And Adenine) with Alkali Metal Ions. Threshold Collision-Induced Dissociation and Theoretical Studies. *J. Am. Chem. Soc.* **2000**, *122*, 8548−8558.
(72) Rajabi, K.; Gillis, E. A. L.; Fridgen, T. D. Structures of Alkali Metal Ion-Adenine Complexes and Hydrated Complexes by IRMPD Spectroscopy and Electronic Structure Calculations. *J. Phys. Chem. A* **2010**, *114*, 3449−3456.

DOI: 10.1021/acs.jpcb.6b06105
J. Phys. Chem. B 2016, 120, 8892−8904